Online Appendix to:

Inflation and Professional Forecast Dynamics: An Evaluation of Stickiness, Persistence, and Volatility*

Elmar Mertens[†] and **James M. Nason**[‡]

February 14, 2018

*This Appendix Contains Supplementary Material Not Intended for Publication.

[†] *email*: elmar.mertens@bis.org, *address*: Bank for International Settlements, Centralbahnplatz 2, CH 4051 Basel, Switzerland.

[‡] *email*: jmnason@ncsu.edu, *address*: Department of Economics, Campus Box 8110, NC State University, Raleigh, NC 27695–8110 and the Centre for Applied Macroeconomic Analysis.

Jim Nason thanks the Jenkins Family Economics Fund at North Carolina State University for financial support. The views herein are those of the authors and do not represent the views of the Bank for International Settlements.

A1 Introduction

This appendix contains four sections. Section A2 builds state space models (SSMs) for the joint data generating process (DGP) of the sticky information (SI) prediction mechanism conditional on different Stock and Watson-unobserved components (SW-UC) models with stochastic volatility (SV). A joint DGP conditional on a SW-UC-SV model with static persistence in gap inflation is developed in section A2.1. Section A2.2 reviews the SSM of the SI-prediction mechanism and SW-UC-SV-TVP-AR(1) model, which is discussed in section 2.3 of the paper. Additional information about the Rao-Blackwellized auxiliary particle filter (RB-APF) of section (3.3) used to estimate the linear and nonlinear state variables of the joint DGP of the SI-prediction mechanism and the SW-UC-SV-TVP-AR(1) model is found in section A3. Estimates of the SSMs left out of the paper appear in section A4. Section A4.1 contains estimates of the SSM that consists of the SI-prediction mechanism and a SW-UC-SV model with no persistence in gap inflation, $\theta_t = 0$. When a static SI parameter, $\lambda_t = \lambda$ is part of the joint DGP, along with the SW-UC-SV-TVP-AR(1) model, the estimates are found in section A4.2.

A2 SSMs of the Joint DGP

The SSMs have several features in common. The features are h-step ahead rational expectations (RE) and SI forecasts, $\mathbf{E}_t\pi_{t+h}$ and $F_t\pi_{t+h}$, are integrated out of the state of the SSMs. Instead, the state vector consists in part of RE and SI inflation trends and gaps, τ_t, ε_t, $F_t\tau_t$, and $F_t\varepsilon_t$. The RE (SI) state variables drive $\mathbf{E}_t\pi_{t+h}$ $(F_t\pi_{t+h})$. Along with these state variables, the SSMs are constructed using the laws of motion of τ_t and ε_t defined by a SW-UC-SV model, and a conjecture for the laws of motion of $F_t\tau_t$ and $F_t\varepsilon_t$ that reflect the SI law of motion, which is equation (3.2) of the paper. Another implication of the SSM

is the RE and SI state variables, $\tau_t \;\; \varepsilon_t, \;\; F_t\tau_t$, and $F_t\varepsilon_t$, are linear conditional on nonlinear state variables. The nonlinear state variables are the SVs of trend and gap inflation, $\varsigma_{\eta,t}$ and $\varsigma_{\upsilon,t}$, drifting inflation gap persistence, θ_t, and the SI-TVP parameter, λ_t, where $\mathcal{V}_t = [\ln\varsigma^2_{\eta,t} \;\; \ln\varsigma^2_{\upsilon,t} \;\; \theta_t \;\; \lambda_t]'$. We gather the conditionally linear state variables together in $\mathcal{X}_t = [\tau_t \;\; \varepsilon_t]'$, $F_t\mathcal{X}_t = [F_t\tau_t \;\; F_t\varepsilon_t]'$, and $\mathcal{S}_t = [\mathcal{X}'_t \;\; F_t\mathcal{X}'_t]'$. The SSM is completed by connecting the observables of realized inflation, π_t, and the average SPF participant's h-step ahead inflation predictions, $\pi^{SPF}_{t,t+h}$ to $\mathcal{S}_t$ plus the associated measurement errors, $\zeta_{\pi,t}$ and $\zeta_{h,t}$, $h = 1, \ldots, \mathcal{H}$. Hence, $\mathbf{E}_t\pi_{t+h}$ and $F_t\pi_{t+h}$ are replaced by the conditionally linear $\mathcal{S}_t$ in the observation equations of $\pi^{SPF}_{t,t+h}$ because these forecasts are linear functions of $\mathcal{X}_t$ and $F_t\mathcal{X}_t$.

A2.1 A SSM of π_t and $\pi^{SPF}_{t,t+h}$ when Persistence in ε_{t+1} Is Fixed

This section constructs a SSM for the joint DGP of the SI-prediction mechanism and a SW-UC-SV model with $\theta_t = \theta$. Our motivation is to study the joint DGP without the complication of specifying a TVP-AR(1) for gap inflation. The restriction is gap inflation evolves as a fixed coefficient AR(1) with SV, where $\varepsilon_{t+1} = \theta\varepsilon_t + \varsigma_{\upsilon,t+1}\upsilon_t$ and $\theta \in (-1, 1)$. In this case, the joint DGP maps into a SSM in which alone λ_t alters the transition dynamics of $F_t\mathcal{X}_t$.

The SSM of the joint DGP is built on RE and SI term structures of inflation. The SW-UC-SV model with fixed inflation gap persistence yields a SSM, which is the source of $\mathbf{E}_t\pi_{t+h}$. We compute $\mathbf{E}_t\pi_{t+h}$ using the observation and state equations of this SSM, which are equation (5.1)

$$\pi_t \;=\; \delta_{\mathcal{X}}\mathcal{X}_t \;+\; \sigma_{\zeta,\pi}\zeta_{\pi,t}, \tag{A2.1}$$

and equation (5.2) modified for fixed inflation gap persistence

$$\mathcal{X}_{t+1} \;=\; \mathbf{\Theta}\mathcal{X}_t \;+\; \mathbf{\Upsilon}_{t+1}\mathcal{W}_t, \tag{A2.2}$$

of the paper, where $\delta_{\mathcal{X}} = [1 \quad 1]$, $\mathbf{\Theta} = \begin{bmatrix} 1 & 0 \\ 0 & \theta \end{bmatrix}$, $\mathbf{\Upsilon}_{t+1} = \begin{bmatrix} \varsigma_{\eta,t+1} & 0 \\ 0 & \varsigma_{\upsilon,t+1} \end{bmatrix}$, and $\mathcal{W}_t = [\eta_t \;\; \upsilon_t]'$. The RE forecast of π_{t+h}, which is equation (6) of the paper (implied hereafter) is reproduced here

$$\mathbf{E}_t \pi_{t+h} \;=\; \delta_{\mathcal{X}} \mathbf{\Theta}^h \mathcal{X}_t, \quad h \;=\; 1, \ldots, \mathcal{H}, \tag{A2.3}$$

Equation (A2.3) is calculated by iterating the observation equation (A2.1) and state equations A2.2 forward h periods, substituting for $\mathcal{X}_{t+h}$ in the former equation using the latter, and applying the law of iterated expectations (LIE).

The SI term structure of inflation forecasts has a similar specification

$$F_t \pi_{t+h} \;=\; \delta_{\mathcal{X}} \mathbf{\Theta}^h F_t \mathcal{X}_t, \tag{A2.4}$$

which is equation (7). This specification is built on the SI-EWMA smoother (4), the RE term structure of inflation forecasts (A2.3), and the EWMA smoother of $F_t \mathcal{X}_t$. Construction of the latter begins by substituting $\delta_{\mathcal{X}} \mathbf{\Theta}^h \mathcal{X}_t$ for $\mathbf{E}_t \pi_{t+h}$ in the SI-EWMA smoother (4) to find

$$F_t \pi_{t+h} \;=\; \delta_{\mathcal{X}} \mathbf{\Theta}^h \sum_{j=0}^{\infty} \mu_{\lambda,t-j} \mathbf{\Theta}^j \left(\prod_{\ell=0}^{j} \lambda_{t-\ell} \right) \mathcal{X}_{t-j}. \tag{A2.5}$$

Next, a law of motion for the SI state vector, $F_{t+1} \mathcal{X}_{t+1}$, is needed to connect it to the RE state vector, $\mathcal{X}_t$. Remember the state variables $\mathcal{X}_t$ and $F_t \mathcal{X}_t$ contain all the information needed to construct the RE and SI term structures of inflation forecasts, which are equations (A2.3) and (A2.4). This information is useful for building a law of motion for the SI state variable. Since the SI law of motion (3.2) relates $F_t \pi_{t+h}$ to its own lag and $\mathbf{E}_t \pi_{t+h}$ weighted by λ_t and $(1 - \lambda_t)$, a law of motion for $F_t \mathcal{X}_{t+h}$ is found by swapping it, $F_{t-1} \mathcal{X}_{t+h}$, and $\mathbf{E}_t \mathcal{X}_{t+h}$ for $F_t \pi_{t+h}$, $F_{t-1} \pi_{t+h}$, and $\mathbf{E}_t \pi_{t+h}$ in the SI law of motion (3.2). The result is the law of motion

$$F_t\mathcal{X}_{t+h} \;=\; \lambda_t F_{t-1}\mathcal{X}_{t+h} \;+\; (1-\lambda_t)\mathbf{E}_t\mathcal{X}_{t+h}. \tag{A2.6}$$

Backward iteration of the SI law of motion (A2.6) yields the EWMA smoother of $F_t\mathcal{X}_{t+h}$

$$F_t\mathcal{X}_{t+h} \;=\; \sum_{j=0}^{\infty} \mu_{\lambda,t-j} \left(\prod_{\ell=0}^{j} \lambda_{t-\ell} \right) \boldsymbol{\Theta}^{h+j}\mathcal{X}_{t-j}, \tag{A2.7}$$

where $\mathbf{E}_{t-j}\mathcal{X}_{t+h} = \boldsymbol{\Theta}^{h+j}\mathcal{X}_{t-j}$. When $h = 0$,

$$F_t\mathcal{X}_{t} \;=\; \sum_{j=0}^{\infty} \mu_{\lambda,t-j} \left(\prod_{\ell=0}^{j} \lambda_{t-\ell} \right) \boldsymbol{\Theta}^{j}\mathcal{X}_{t-j}, \tag{A2.8}$$

which establishes the link between $F_t\pi_{t+h}$ and $F_t\mathcal{X}_t$ in the SI inflation term structure (A2.4).

We employ the state equations (A2.2) of $\mathcal{X}_{t+1}$ and the SI-EWMA smoother (A2.8) to build state equations for $F_{t+1}\mathcal{X}_{t+1}$. By pulling $\mathcal{X}_t$ out of the infinite sum of the SI-state equation EWMA smoother (A2.8), the result is

$$F_t\mathcal{X}_{t} \;=\; (1-\lambda_t)\mathcal{X}_t \;+\; \sum_{j=1}^{\infty} \mu_{\lambda,t-j} \left(\prod_{\ell=0}^{j} \lambda_{t-\ell} \right) \boldsymbol{\Theta}^{j}\mathcal{X}_{t-j}. \tag{A2.9}$$

The infinite sum of equation (A2.9) implies $F_{t-1}\mathcal{X}_{t-1} = \sum_{i=0}^{\infty} \mu_{\lambda,t-i-1} \left(\prod_{\ell=0}^{i} \lambda_{t-\ell} \right) \boldsymbol{\Theta}^{i+1}\mathcal{X}_{t-i-1}$ after a change of index, $j = i+1$. Substitute for the infinite sum in equation (A2.9) with $F_{t-1}\mathcal{X}_{t-1}$ to produce

$$F_t\mathcal{X}_{t} \;=\; (1-\lambda_t)\mathcal{X}_t \;+\; \lambda_t\boldsymbol{\Theta}F_{t-1}\mathcal{X}_{t-1}. \tag{A2.10}$$

The goal of finding the law of motion is almost complete. Subsequent to leading the law of motion (A2.10) forward one period and substituting for $\mathcal{X}_{t+1}$ using the state equations (A2.2), we have the SI state equations

$$F_{t+1}\mathcal{X}_{t+1} \;=\; \lambda_{t+1}\boldsymbol{\Theta}F_t\mathcal{X}_t \;+\; (1-\lambda_{t+1})\boldsymbol{\Theta}\mathcal{X}_t \;+\; (1-\lambda_{t+1})\boldsymbol{\Upsilon}_{t+1}\mathcal{W}_t, \tag{A2.11}$$

of the joint DGP of the SI prediction mechanism and the SW-UC-SV model with fixed inflation gap persistence. The state equations (A2.2) of $\mathcal{X}_{t+1}$ are stacked on top of the

state equations (A2.11) of $F_{t+1}\mathcal{X}_{t+1}$ to form

$$\mathcal{S}_{t+1} = \mathcal{A}_{\Theta,t+1}\mathcal{S}_t + \mathcal{B}_{t+1}\mathcal{W}_t, \tag{A2.12}$$

where $\mathcal{A}_{\Theta,t+1} = \begin{bmatrix} \Theta & \mathbf{0}_{2\times 2} \\ \left(1-\lambda_{t+1}\right)\Theta & \lambda_{t+1}\Theta \end{bmatrix}$, and $\mathcal{B}_{t+1} = \begin{bmatrix} \Upsilon_{t+1} \\ \left(1-\lambda_{t+1}\right)\Upsilon_{t+1} \end{bmatrix}$. Thus, the system of state equations (A2.12) of the joint DGP reveal shocks to λ_{t+1} alone shift the transition dynamics of $F_{t+1}\mathcal{X}_{t+1}$ and its impulse dynamics react to λ_{t+1} and SVs.

The SSM of the joint DGP of the SI prediction mechanism and the SW-UC-SV model with fixed inflation gap persistence is finished by using equations (A2.1) and (3.1) to construct the system of observation equations

$$\mathcal{Y}_t = \mathcal{C}_\Theta \mathcal{S}_t + \mathcal{D}\mathcal{U}_t, \tag{A2.13}$$

where $\mathcal{Y}_t = \begin{bmatrix} \pi_t \\ \pi_{1,t}^{SPF} \\ \vdots \\ \pi_{\mathcal{H},t}^{SPF} \end{bmatrix}$, $\mathcal{C}_\Theta = \begin{bmatrix} \delta_\mathcal{X} & \mathbf{0}_{1\times 2} \\ \mathbf{0}_{1\times 2} & \delta_\mathcal{X}\Theta \\ \vdots & \vdots \\ \mathbf{0}_{1\times 2} & \delta_\mathcal{X}\Theta^\mathcal{H} \end{bmatrix}$, $\mathcal{D} = \begin{bmatrix} \sigma_{\zeta,\pi} & 0 & \dots & 0 \\ 0 & \sigma_{\zeta,1} & \dots & 0 \\ 0 & 0 & \ddots & 0 \\ 0 & 0 & \dots & \sigma_{\zeta,\mathcal{H}} \end{bmatrix}$, $\mathcal{U}_t = \begin{bmatrix} \zeta_{\pi,t} & \zeta_{1,t} & \dots & \zeta_{\mathcal{H},t} \end{bmatrix}'$, and $\Omega_\mathcal{U} = \mathcal{D}\mathcal{D}'$. The SPF term structure of inflation predictions are the second through $\mathcal{H}+1$ rows of the observation equations (A2.13). These observation equations show $F_t\pi_{t+h}$ is integrated out of the SSM and that the factor loadings on $\mathcal{S}_t$ are time invariant.

A2.2 The Joint DGP with Drifting Persistence in Gap Inflation

The SSM of the SI-prediction mechanism and SW-UC-SV-TVP-AR(1) model is more difficult to construct compared with the SSM of the previous section. The difficulty stems from drifting persistence in gap inflation, which creates a nonlinearity in the transition dynamics of the state equations (5.2) of the SW-UC-SV-TVP-AR(1) model. This nonlin-

earity rule outs using the LIE to compute $\mathbf{E}_t \pi_{t+h}$. Instead, the anticipated utility model (AUM) is employed to solve the problem. Under the AUM assumptions stated in the paper, the average member of the SPF holds $\mathbf{\Theta}_{t+h}$ fixed at its date t realization when constructing h-step ahead inflation forecasts. For example, combine the AUM and procedures similar to ones used to construct the RE term structure of inflation (A2.3) under fixed inflation gap persistence generates the forecasts

$$\mathbf{E}_t \pi_{t+h} = \delta_{\mathcal{X}} \mathbf{\Theta}_{t|t}^{h} \mathcal{X}_t, \tag{A2.14}$$

where $\mathbf{\Theta}_t = \begin{bmatrix} 1 & 0 \\ 0 & \theta_t \end{bmatrix}$. The subscript on $\mathbf{\Theta}_{t|t}$ is held fixed in the RE term structure of inflation (A2.14) to reflect information available to evaluate the SW-UC-SV-TVP-AR(1) model at date t.

The SI term structure of inflation forecasts also has to be calculated to build the SSM of the joint DGP. Similar to the previous section, the process of computing these forecasts starts with the law of motion (A2.6) of $F_t \mathcal{X}_{t+h}$, $(1 - \lambda_t)\mathbf{E}_t \mathcal{X}_{t+h} + \lambda_t F_{t-1} \mathcal{X}_{t+h}$, and its EWMA smoother (A2.7), $\sum_{j=0}^{\infty} \mu_{\lambda,t-j} \left(\prod_{\ell=0}^{j} \lambda_{t-\ell} \right) \mathbf{E}_{t-j} \mathcal{X}_{t+h}$. Although this law of motion and smoother are unchanged from the case of $\theta_t = \theta$, drift in inflation gap persistence matters for constructing the map from $\mathbf{E}_{t-j} \mathcal{X}_{t+h}$ to $F_t \mathcal{X}_t$. Similar to the implication of AUM, which holds drifting inflation gap persistence fixed at $\theta_{t|t}$ to generate the h-step ahead RE inflation forecast (A2.14), we assume θ_t is fixed conditional on the information available to $F_t \mathcal{X}_{t+h}$. Thus, iterating the law of motion (A2.6) of $F_t \mathcal{X}_{t+h}$ backwards gives

$$F_t \mathcal{X}_{t+h} = \sum_{j=0}^{\infty} \mu_{\lambda,t-j} \left(\prod_{\ell=0}^{j} \lambda_{t-\ell} \right) \mathbf{\Theta}_{t|t}^{h+j} \mathcal{X}_{t-j}, \tag{A2.15}$$

which is implied by the RE term structure of inflation forecasts (A2.14), $\mathbf{E}_{t-j} \pi_{t+h} =$

$\mathbf{\Theta}_{t|t}^{h+j}\mathcal{X}_{t-j}$. Next, set $h = 0$ in the EWMA (A2.15) of $F_t\mathcal{X}_{t+h}$ to obtain

$$F_t\mathcal{X}_t = \sum_{j=0}^{\infty} \mu_{\lambda,t-j} \left(\prod_{\ell=0}^{j} \lambda_{t-\ell} \right) \mathbf{\Theta}_{t|t}^{j} \mathcal{X}_{t-j}. \tag{A2.16}$$

Apply the EWMA (A2.16) of $F_t\mathcal{X}_t$ to link the SI-EWMA smoother (4) to the h-step ahead RE inflation forecast (A2.14) yields

$$F_t\pi_{t+h} = \delta_{\mathcal{X}} \sum_{j=0}^{\infty} \mu_{\lambda,t-j} \left(\prod_{\ell=0}^{j} \lambda_{t-\ell} \right) \mathbf{\Theta}_{t|t}^{h+j} \mathcal{X}_{t-j}. \tag{A2.17}$$

The SI term structure of inflation forecasts

$$F_t\pi_{t+h} = \delta_{\mathcal{X}} \mathbf{\Theta}_{t|t}^{h} F_t\mathcal{X}_t, \tag{A2.18}$$

is an implication of the SI-EWMA smoothers (A2.16) of $F_t\pi_{t+h}$ and (A2.16) of $F_t\mathcal{X}_t$.

The SI-EWMA smoother (A2.16) of $F_t\mathcal{X}_t$ also contributes to the state equations of $F_{t+1}\mathcal{X}_{t+1}$. Unwinding the infinite sum of (A2.16) gives the recursion

$$F_t\mathcal{X}_t = (1 - \lambda_t)\mathcal{X}_t + \lambda_t \mathbf{\Theta}_{t|t} F_{t-1}\mathcal{X}_{t-1}. \tag{A2.19}$$

Lead the law of motion (A2.19) of $F_t\mathcal{X}_t$ by one period and substitute for $\mathcal{X}_{t+1}$ using the state equations (5.2) to produce

$$F_{t+1}\mathcal{X}_{t+1} = (1 - \lambda_{t+1})\mathbf{\Theta}_{t+1}\mathcal{X}_t + \lambda_{t+1}\mathbf{\Theta}_{t+1}F_t\mathcal{X}_t + (1 - \lambda_{t+1})\mathbf{\Upsilon}_{t+1}\mathcal{W}_t, \tag{A2.20}$$

where we drop the conditioning time subscript on $\mathbf{\Theta}_{t+1}$. Equations (A2.20) duplicate the bottom two rows of the state equations (8.1). The timing of the conditionally linear and nonlinear state variables on the right hand side of the state equations (A2.20) appear nonstandard. However, the timing conventions of these state equations are consistent with the specification of the hierarchical conditional linear Gaussian (CLG) model studied by Lindsten, Bunch, Särkkä, Schön, and Godsill (2016). They develop a

particle smoother for the CLG model that we employ to generate smoothed estimates of the linear and nonlinear state variables of the SSMs of this and the previous section. Thus, our use of the Lindsten et al particle smoother is supported by the AUM assumptions and the assumption that θ_{t+1} is held fixed at its current realization when iterating backwards to construct SI-EWMA smoothers.

A3 Econometric Methods

We estimate the SSM (8.1) and (8.2) using Bayesian sequential Monte Carlo (SMC) methods. The methods combine Rao-Blackwellization (RB) of the SSM with the auxiliary particle filter (APF) of Pitt and Shephard (1999, 2001) to estimate the linear and nonlinear state variables. Our RB-APF algorithm is adapted from a version outlined by Creal (2012) and algorithm 2 Lopes and Tsay (2011, p. 173). Estimates of the static scale volatility coefficients are produced with the particle learning estimator (PLE) of Storvik (2002); also see Carvalho, Johannes, Lopes, and Polson (2010). The next section gives details about running the RB-APF that is sketched in section 3.3 of our paper.

A3.1 The RB-APF Algorithm

The RB-APF of section (3.3) produces M filtered estimates of the linear states, $\mathcal{S}_t$, its mean square error (MSE), $\boldsymbol{\Sigma}_t$, and the nonlinear states, $\mathcal{V}_{t+1}$. The Kalman filter (KF) is the source of estimates of $\mathcal{S}_t$ and $\boldsymbol{\Sigma}_t$ particle by particle while M synthetic samples of $\mathcal{V}_{t+1}$ are generated by simulating the multivariate random walk (9). The predictive step of the KF yields M estimates of the likelihood that are the source of the weights used to resample the M particles of $\mathcal{S}_t$, $\boldsymbol{\Sigma}_t$, and $\mathcal{V}_{t+1}$. Conditioning on the resampled $\mathcal{S}_t$, $\boldsymbol{\Sigma}_t$, and $\mathcal{V}_{t+1}$, running the KF produces updates of the linear states.

We carry out the RB-APF algorithm in the following steps.

1. Initialize the filter with $i = 1, \ldots, M$ particle draws of $\mathcal{V}_0^{(i)}$ sampled from the priors specified in table 2:

$$\begin{aligned}
\ln \varsigma_{\eta,0}^{2\,(i)} &\sim \ln \mathcal{N}\left(\ln\left(\overline{\varsigma}_{\eta,0}^2\right) - \frac{\sigma_{\varsigma_\eta,0}^2}{2},\, \sigma_{\varsigma_\eta,0}^2\right), \\
\ln \varsigma_{\upsilon,0}^{2\,(i)} &\sim \ln \mathcal{N}\left(\ln\left(\overline{\varsigma}_{\upsilon,0}^2\right) - \frac{\sigma_{\varsigma_\upsilon,0}^2}{2},\, \sigma_{\varsigma_\upsilon,0}^2\right), \\
\theta_0^{(i)} &\sim \mathcal{TN}\left(\overline{\theta}_0,\, \sigma_{\phi,0}^2,\, -1.0,\, 1.0\right), \\
\text{and} \quad \lambda_0^{(i)} &\sim \mathcal{TN}\left(\overline{\lambda}_0,\, \sigma_{\kappa,0}^2,\, 0.0,\, 1.0\right),
\end{aligned}$$

   where $\mathcal{TN}$ denotes the truncated normal distribution, the prior means $\overline{\varsigma}_{\eta,0}^2 = 0.2$, $\overline{\varsigma}_{\upsilon,0}^2 = 0.4$, $\overline{\theta}_0 = 0$, $\overline{\lambda}_0 = 0.5$ and prior variances $\sigma_{\varsigma_\eta,0}^2 = \sigma_{\varsigma_\upsilon,0}^2 = 10.0$ and $\sigma_{\phi,0}^2 = \sigma_{\kappa,0}^2 = 1.0$ are listed in table 2 and conditional on $\mathcal{V}_0^{(i)}$ draw $\mathcal{S}_0 \sim \mathcal{N}\left(\mathcal{S}_{0|0}^{(i)}, \boldsymbol{\Sigma}_{0|0}^{(i)}\right)$. In addition, let $\beta_{\ell,0}^{(i)} = \beta_\ell \;\forall i = 1, 2, \ldots M$ where β_ℓ is the shape parameter of the inverse gamma ($\mathcal{IG}$) priors for $\ell = \eta,\ \upsilon$, ϕ, and κ, displayed in table 1.

2. Draw inital particle values for the static scale paramters $\sigma_\ell^{(i)} \sim \sqrt{\mathcal{IG}\left(\alpha_\ell/2, \beta_{\ell,t}^{(i)}/2\right)}$ for $\ell = \eta,\ \upsilon$, ϕ, and κ, as well as $(\zeta, \pi), (\zeta, 1), \ldots, (\zeta, \mathcal{H})$.

3. Repeat the following steps for $t = 1, \ldots, T$, where each step uses the particles $\mathcal{V}_{t-1}^{(i)}$, $\sigma_\ell^{(i)}$, $\mathcal{S}_{t-1|t-1}^{(i)}$, and $\boldsymbol{\Sigma}_{t-1|t-1}^{(i)}$, obtained before.

   (a) Auxiliary particle step: For $i = 1, 2, \ldots, M$, use the median predictions of the lagged particles as auxiliary proposals for time t by setting $\mathcal{V}_t^{(i)}$ equal to $\mathcal{V}_{t-1}^{(i)}$ and engage the following KF predictive step to compute

$$
\begin{aligned}
\mathcal{S}_{t|t-1}^{(i)} &= \mathcal{A}_t^{(i)} \mathcal{S}_{t-1|t-1}^{(i)}, \\
\boldsymbol{\Sigma}_{t|t-1}^{(i)} &= \mathcal{A}_t^{(i)} \boldsymbol{\Sigma}_{t-1|t-1}^{(i)} \left(\mathcal{A}_t^{(i)}\right)' + \mathcal{B}_t^{(i)} \left(\mathcal{B}_t^{(i)}\right)', \\
\boldsymbol{\Omega}_{t|t-1}^{(i)} &= \mathcal{C}_t^{(i)} \boldsymbol{\Sigma}_{t|t-1}^{(i)} \left(\mathcal{C}_t^{(i)}\right)' + \boldsymbol{\Omega}_{\mathcal{U}}^{(i)}, \\
\widetilde{\mathcal{Y}}_t^{(i)} &= \mathcal{Y}_t - \mathcal{C}_t^{(i)} \mathcal{S}_{t|t-1}^{(i)}, \\
\ell_t^{(i)} &= -\frac{1}{2}\left[\ln\left|\boldsymbol{\Omega}_{t|t-1}^{(i)}\right| + \left(\widetilde{\mathcal{Y}}_t^{(i)}\right)' \left(\boldsymbol{\Omega}_{t|t-1}^{(i)}\right)^{-1} \widetilde{\mathcal{Y}}_t^{(i)}\right],
\end{aligned}
$$

across the M auxiliary particles, $i = 1, 2, \ldots, M$.[A.1]

(b) Compute auxiliary particle weights $\widehat{\omega}_t^{(i)} = \dfrac{\exp\left\{\ell_t^{(i)}\right\}}{\sum_{i=1}^{M} \exp\left\{\ell_t^{(i)}\right\}}$.

(c) Auxiliary resampling: Shuffle the index i=1, …, M by drawing from a multinominal distribution using the *pdf* of $\widehat{\omega}_t^{(i)}$, which is stratified resampling of the original particles obatined at time $t-1$: $\mathcal{V}_{t-1}^{(i)}$, $\beta_{\ell,t-1}^{(i)}$, $\mathcal{S}_{t-1|t-1}^{(i)}$, and $\boldsymbol{\Sigma}_{t-1|t-1}^{(i)}$, where $\ell = \eta,\ \upsilon,\ \phi$, and κ; see Hol, Schön, and Gustafsson (2006) for details.

(d) For $i = 1, 2, \ldots, M$, draw new particles $\mathcal{V}_t^{(i)}$ conditional on the resampled values for $\mathcal{V}_{t-1}^{(i)}$ and the law of motion (12) using

$$
\begin{aligned}
\ln \varsigma_{\eta,t}^{2\,(i)} &= \ln \varsigma_{\eta,t-1}^{2\,(i)} + \sigma_\eta^{(i)} \eta_t^{(i)} \\
\ln \varsigma_{\upsilon,t}^{2\,(i)} &= \ln \varsigma_{\upsilon,t-1}^{2\,(i)} + \sigma_\upsilon^{(i)} \upsilon_t^{(i)} \\
\theta_t^{(i)} &\sim \mathcal{TN}\left(\theta_{t-1}^{(i)},\ \sigma_{\phi,}^{(i)},\ -1.0,\ 1.0\right) \\
\text{and} \quad \lambda_t^{(i)} &\sim \mathcal{TN}\left(\lambda_{t-1}^{(i)},\ \sigma_\kappa^{(i)},\ 0.0,\ 1.0\right)
\end{aligned}
$$

where $\eta_t^{(i)}$ and $\upsilon_t^{(i)}$ represent draws from standard normal distributions.

[A.1] There are missing observations in the SPF inflation data that the KF handles using standard methods.

(e) For $\ell = \eta,\ \upsilon, \phi$, and κ, update sufficient statistics for the static scale parameters $\beta_{\ell,t}^{(i)} = \beta_{\ell,t-1}^{(i)} + \left(\Delta_{\ell,t}^{(i)}\right)^2$. Where $\Delta_{\ell,t}^{(i)}$ denotes the increments from updating the non-linear state variables in step (d): $\Delta_{\eta,t}^{(i)} = \sigma_{\eta,t}^{(i)} \eta_t^{(i)}$, $\Delta_{\upsilon,t}^{(i)} = \sigma_{\upsilon,t}^{(i)} \upsilon_t^{(i)}$, $\Delta_{\phi,t}^{(i)}$ $= d\mathcal{IN}_{\phi,t}^{(i)}$, and $\Delta_{\kappa,t}^{(i)} = d\mathcal{IN}_{\kappa,t}^{(i)}$.

(f) Given particles $\left\{\mathcal{V}_t^{(i)},\ \beta_{\ell,t}^{(i)}, \mathcal{S}_{t-1|t-1}^{(i)},\ \boldsymbol{\Sigma}_{t-1|t-1}^{(i)}\right\}_{i=1}^{M}$, run the KF

$$
\begin{aligned}
\mathcal{S}_{t|t-1}^{(i)} &= \boldsymbol{\mathcal{A}}_t^{(i)} \mathcal{S}_{t-1|t-1}^{(i)}, \\
\boldsymbol{\Sigma}_{t|t-1}^{(i)} &= \boldsymbol{\mathcal{A}}_t^{(i)} \boldsymbol{\Sigma}_{t-1|t-1}^{(i)} \left(\boldsymbol{\mathcal{A}}_t^{(i)}\right)' + \boldsymbol{\mathcal{B}}_t^{(i)} \left(\boldsymbol{\mathcal{B}}_t^{(i)}\right)', \\
\boldsymbol{\Omega}_{t|t-1}^{(i)} &= \mathcal{C}_t^{(i)} \boldsymbol{\Sigma}_{t|t-1}^{(i)} \left(\mathcal{C}_t^{(i)}\right)' + \boldsymbol{\Omega}_{\mathcal{U}}^{(i)}, \\
\tilde{\mathcal{Y}}_t^{(i)} &= \mathcal{Y}_t - \mathcal{C}_t^{(i)} \mathcal{S}_{t|t-1}^{(i)}, \\
\mathcal{K}_t^{(i)} &= \boldsymbol{\Sigma}_{t|t-1}^{(i)} \left(\mathcal{C}_t^{(i)}\right)' \left(\boldsymbol{\Omega}_{t|t-1}^{(i)}\right)^{-1}, \\
\mathcal{S}_{t|t}^{(i)} &= \boldsymbol{\mathcal{A}}_t^{(i)} \mathcal{S}_{t|t-1}^{(i)} + \mathcal{K}_t^{(i)} \tilde{\mathcal{Y}}_t^{(i)}, \\
\boldsymbol{\Sigma}_{t|t}^{(i)} &= \boldsymbol{\Sigma}_{t|t-1}^{(i)} - \boldsymbol{\Sigma}_{t|t-1}^{(i)} \left(\mathcal{C}_t^{(i)}\right)' \left(\boldsymbol{\Omega}_{t|t-1}^{(i)}\right)^{-1} \mathcal{C}_t^{(i)} \boldsymbol{\Sigma}_{t|t-1}^{(i)}, \\
\ell_t^{(i)} &= -\frac{1}{2}\left[\ln\left|\boldsymbol{\Omega}_{t|t-1}^{(i)}\right| + \left(\tilde{\mathcal{Y}}_t^{(i)}\right)' \left(\boldsymbol{\Omega}_{t|t-1}^{(i)}\right)^{-1} \tilde{\mathcal{Y}}_t^{(i)}\right], \\
\omega_t^{(i)} &= \frac{\exp\left\{\ell_t^{(i)}\right\}}{\sum_{i=1}^{M} \exp\left\{\ell_t^{(i)}\right\}},
\end{aligned}
$$

particle by particle to create updates of $\mathcal{S}_{t|t}^{(i)}$, $\boldsymbol{\Sigma}_{t|t}^{(i)}$, and $\ell_t^{(i)}$, and new weights $\omega_t^{(i)}$, which are used to resample $\left\{\mathcal{V}_t^{(i)}\right\}_{i=1}^{M}$.

(g) For $\ell = \pi, 1, 2, \ldots, \mathcal{H}$, update sufficient statistics for the static measurement error variance parameters $\beta_{(\zeta,\ell),t}^{(i)} = \beta_{(\zeta,\ell),t-1}^{(i)} + \left(\Delta_{(\zeta,\ell),t}^{(i)}\right)^2$. Where

$$
\Delta_{(\zeta,\ell),t}^{(i)} = h_\ell \tilde{\mathcal{Y}}_t^{(i)} \cdot \sqrt{\frac{h_\ell \boldsymbol{\Omega}_{\mathcal{U}}^{(i)} h_\ell'}{h_\ell \boldsymbol{\Omega}_{t|t-1}^{(i)} h_\ell'}}
$$

denotes the scaled innovations to the Kalman filter's observer equations, and

h_ℓ is a selection vector that picks out the suitable element of $\widetilde{\mathcal{Y}}_t^{(i)}$.

4. Conditional on $\mathcal{V}_t$, $\mathcal{Y}_{1:t}$, and Ψ, the filtered distribution of $\mathcal{V}_{t+1}$ is approximated by the discrete distribution of particles $\mathcal{V}_{t+1}^{(i)}$ using the *pdf* of $\widetilde{\omega}_t^{(i)}$, where $\widetilde{\omega}_t^{(i)} = \frac{\omega_t^{(i)}}{\widehat{\omega}_t^{(i)}}$, and the associated filtered distribution of $\mathcal{S}_t$ is approximated by a mixture of normals $\mathcal{N}\left(\mathcal{S}_{t|t}^{(i)}, \boldsymbol{\Sigma}_{t|t}^{(i)}\right)$. Thus, the filtered means of $\mathcal{S}_t$ and $\mathcal{V}_{t+1}$ are approximated by $\mathcal{S}_{t|t} = \sum_{i=1}^{M} \widetilde{\omega}_t^{(i)} \mathcal{S}_{t|t}^{(i)}$ and $\mathcal{V}_{t+1|t+1} = \sum_{i=1}^{M} \widetilde{\omega}_t^{(i)} \mathcal{V}_{t+1}^{(i)}$.

5. Store conditional moments $\mathcal{S}_{t|t}^{(i)}$ and $\boldsymbol{\Sigma}_{t|t}^{(i)}$ and particle draws $\mathcal{V}_{t+1}^{(i)}$ to report estimates of the joint DGP of the SI-prediction mechanism and SW-UC-SV-TVP-AR(1) model.

6. Resample particles $\mathcal{V}_t^{(i)}$, $\beta_{\ell,t}^{(i)}$, $\mathcal{S}_{t|t}^{(i)}$, and $\boldsymbol{\Sigma}_{t|t}^{(i)}$, where $\ell = \eta,\ \upsilon,\ \phi$, and κ using stratified resampling with the *pdf* $\widehat{\omega}_t^{(i)}$.

7. Draw new particle values for the static scale parameters $\sigma_\ell^{(i)} \sim \sqrt{\mathcal{IG}\left(t_\nu/2, \beta_{\ell,t}^{(i)}/2\right)}$ with $t_\nu = t + \alpha_\ell$ for $\ell = \eta,\ \upsilon,\ \phi$, and κ, as well as $(\zeta, \pi), (\zeta, 1), \ldots, (\zeta, \mathcal{H})$.

The RB-APF algorithm is straightforward to adapt to gap inflation lacking persistence or to a fixed SI parameter. In the former case, the nonlinear state vector $\mathcal{V}_{t+1}$ drops θ_t and σ_ϕ^2 is deleted from Ψ. Otherwise, the algorithm described above is unchanged. Fixing the SI parameter, $\lambda_t = \lambda$, has a larger impact on the RB-APF algorithm. Besides cutting λ_t out of $\mathcal{V}_{t+1}$ and σ_κ^2 from Ψ, a prior is needed for λ. The posterior for λ has to be analytic for the prior to satisfy the demands of the particle learning estimator (PLE). Another restriction to satisfy is $\lambda \in (0, 1)$. A beta distribution fulfills the requirements of the PLE and the restriction on λ, given the shape parameters equal one (*i.e.*, a uniform distribution on the open unit interval). The RB-APF algorithm is further adjusted by including λ in Ψ, given the beta prior attached to λ.

A4 Additional Results

This section presents estimates of the joint DGPs not discussed in the paper. The estimates are displayed in figures that are similar to ones contained in the paper. However, figure 1 is not reproduced here because it depicts realized inflation, the SPF nowcast and 1-, 2-, and 4-quarter ahead SPF inflation predictions.

A4.1 Estimates of the Joint DGP when $\theta_t = 0$

Estimates of the joint DGP of the SI-prediction mechanism and SW-UC-SV model with zero or no gap inflation persistence, $\theta_t = 0$, appear in figures A2–No Gap Persistence, A3–No Gap Persistence, A4–No Gap Persistence, and A7–No Gap Persistence. This numbering matches figures 2, 3, 4, and 7 of the paper. Hence, conditional on $\theta_t = 0$, this section presents estimates of the scale volatility parameters σ_η^2, σ_υ^2, and σ_κ^2 in figure A2–No Gap Persistence, filtered RE and SI trend and gap inflation, $\tau_{t|t}$, $F_{t|t}\tau_t$, $\varepsilon_{t|t}$, and $F_{t|t}\varepsilon_t$, in figure A3–No Gap Persistence, filtered and smoothed trend and gap inflation SVs, $\varsigma_{\eta,t|t}$, $F_{t|t}\varsigma_{\eta,t}$, $\varsigma_{\upsilon,t|t}$, and $F_{t|t}\varsigma_{\upsilon,t}$, in figure A4–No Gap Persistence, and the volatility of RE and SI trend inflation, τ_t and $F_t\tau_t$, conditional on different information sets in figure A7–No Gap Persistence.

Restricting ε_t to have zero persistence in the joint DGP produces four key differences compared with estimates of the joint DGP when there is drifting persistence in gap inflation. First, estimates of σ_η^2, σ_υ^2, and σ_κ^2 in figure A2–No Gap Persistence are smooth compared with the estimates found in figures 2(a), 2(b), and 2(d). Second, figures A3(a) and A3(b)–No Gap Persistence plot $\tau_{t|t}$ and $F_{t|t}\tau_t$ that are closer to $\pi_{t,t+1}^{SPF}$ and $\pi_{t,t+5}^{SPF}$ than produced by the joint DGP of the SI-prediction mechanism and SW-UC-SV-TVP-AR(1) model, which are plotted in figures 3(a) and 3(b). The implication is $\varepsilon_{t|t}$ and $F_{t|t}\varepsilon_t$, which are seldom greater than two percent and are displayed in figure A3(d)-No

Gap Persistence, are less than a third as volatile compared with the estimates of RE and SI gap inflation shown in figure A3(d). Next, when $\theta_t = 0$, $\varsigma_{\eta,t|t}$ and $F_{t|t}\varsigma_{\eta,t}$ have similar peaks around the 1973–1975 and 1981–1982 recessions figures A4(a) and A4(b)–No Gap Persistence. This differs from the peaks in $\varsigma_{\eta,t|t}$ and $F_{t|t}\varsigma_{\eta,t}$ that occur during the latter recession in figures 4(a) and 4(b). Subsequently, $\varsigma_{\eta,t|t}$ and $F_{t|t}\varsigma_{\eta,t}$ decline through the restr of the sample period, except for a small spike around the 2007–2009 recession, in figures A4(a) and A4(b)–No Gap Persistence. Figures 4(c) and (d) and A4(c) and A4(d)–No Gap Persistence have qualitatively similar estimates of $\varsigma_{\upsilon,t|t}$ and $F_{t|t}\varsigma_{\upsilon,t}$ in that all these plots show a peak during the 1973–1975 recession. Lastly, estimates of the volatility of τ_t and $F_t\tau_t$ are qualitatively similar in figures 7 and A7–No Gap Persistence. However, conditioning only on realized inflation, π_t, yields lower estimates of the volatility of τ_t and $F_t\tau_t$, given $\theta_t = 0$, compared with the corresponding estimates in figure 7.

Figure A2–No Gap Persistence: Estimates of Static Volatility Parameters, 1968$Q4$ to 2017$Q2$

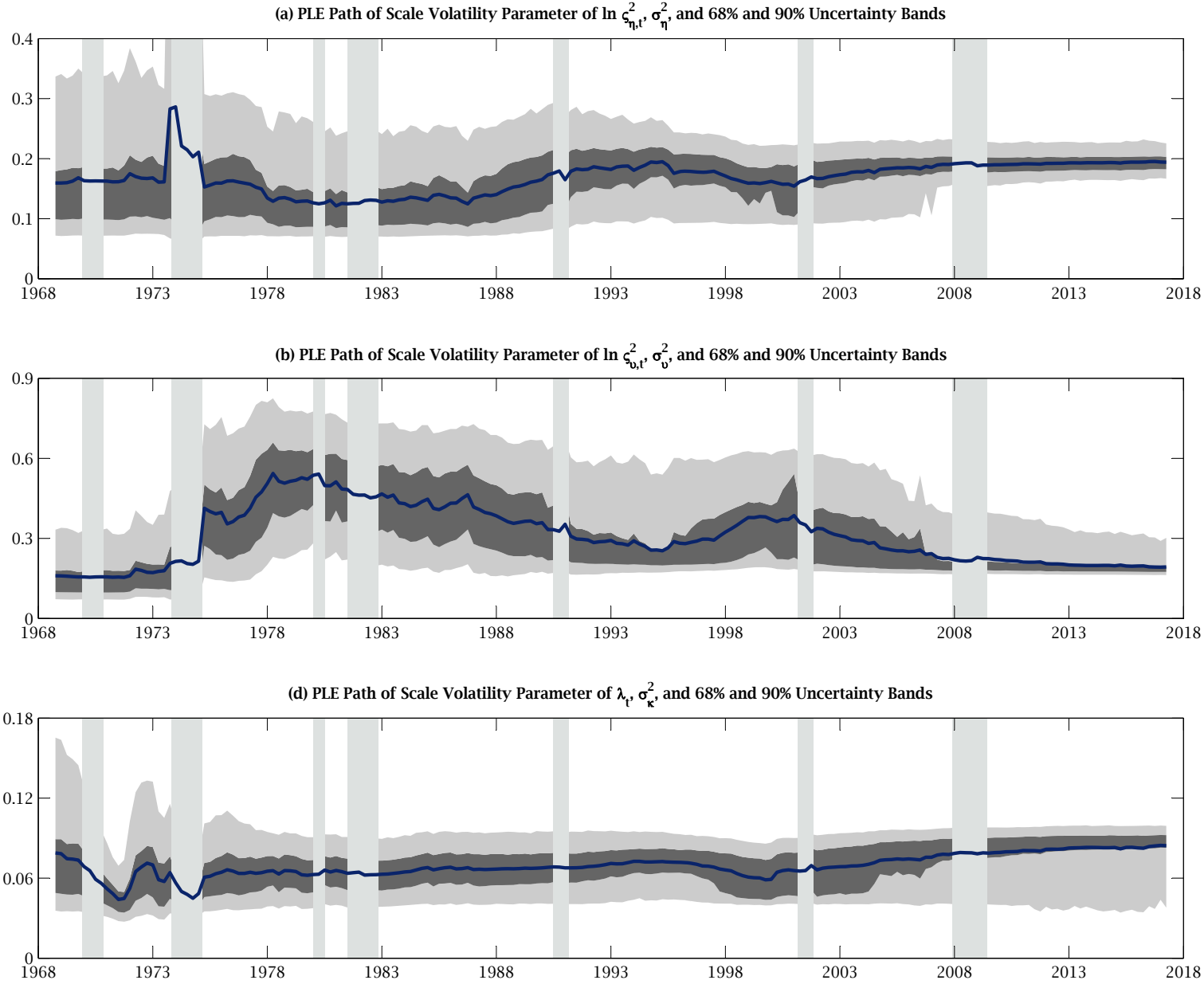

Note: The static volatility parameters are estimated in a joint DGP in which gap inflation, ε_t, has no persistence. The dark (light) gray areas surrounding estimates of the static scale volatility parameters, σ^2_η, σ^2_υ, and σ^2_κ cover 68 (90) percent uncertainty bands. The four plots contain vertical gray bands that denote NBER dated recessions.

Figure A3–No Gap Persistence: Realized Inflation, SPF Inflation Predictions, and Estimates of Trend and Gap Inflation, 1968$Q4$ to 2017$Q2$

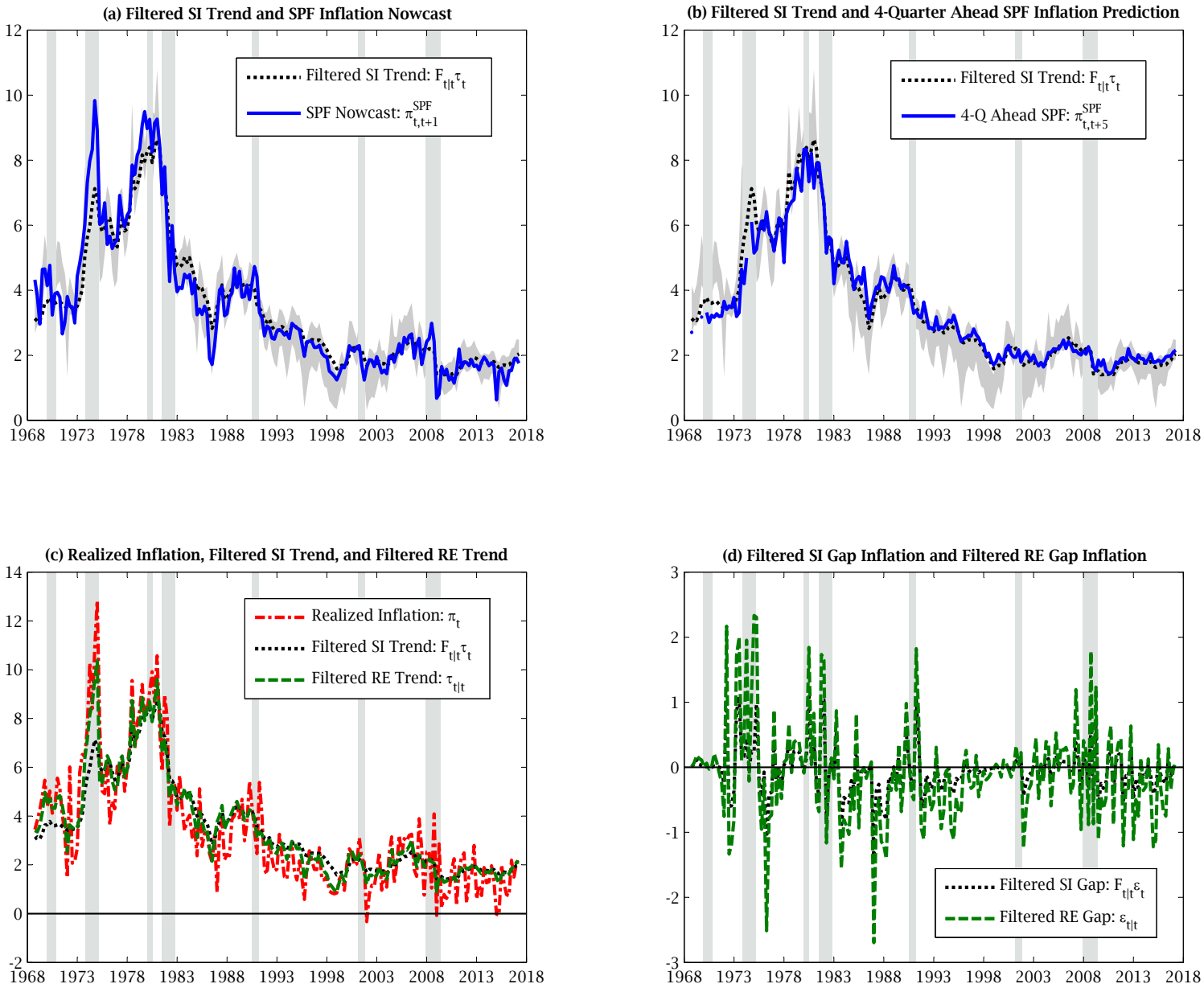

Note: The filtered RE and SI inflation trends and gaps are estimated in a joint DGP in which gap inflation, ε_t, has no persistence. The top row of charts contains light gray shaded areas that represent 68 percent uncertain bands around estimates of filtered SI trend inflation, $F_{t|t}\tau_t$. The vertical gray bands denote NBER dated recessions in the four charts.

Figure A4–No Gap Persistence: Estimates of the Stochastic Volatility of Trend and Gap Inflation, 1968$Q4$ to 2017$Q2$

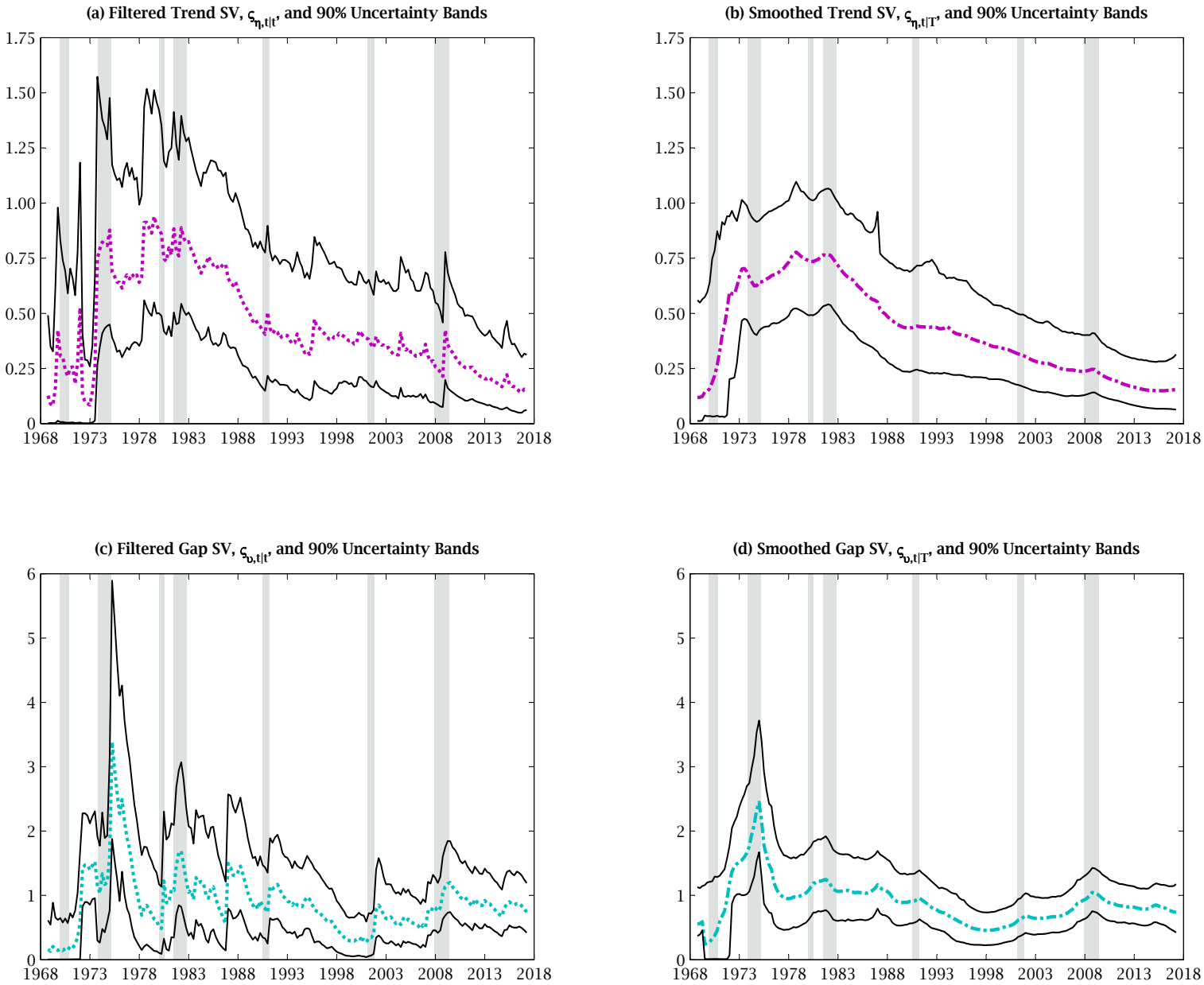

Note: The filtered and smoothed SVs of trend and gap inflation, $\varsigma_{\eta,t|t}$ and $\varsigma_{\eta,t|T}$, are estimated in a joint DGP in which gap inflation, ε_t, has no persistence. The solid thin (black) lines around $\varsigma_{\eta,t|t}$ and $\varsigma_{\eta,t|T}$ are lower and upper bounds on 90 percent uncertainty bands. The four plots display vertical gray bands that denote NBER dated recessions.

Figure A7–No Gap Persistence: Uncertainty Measure of Trend Inflation Conditional on Different Information Sets, 1968$Q4$ to 2017$Q2$

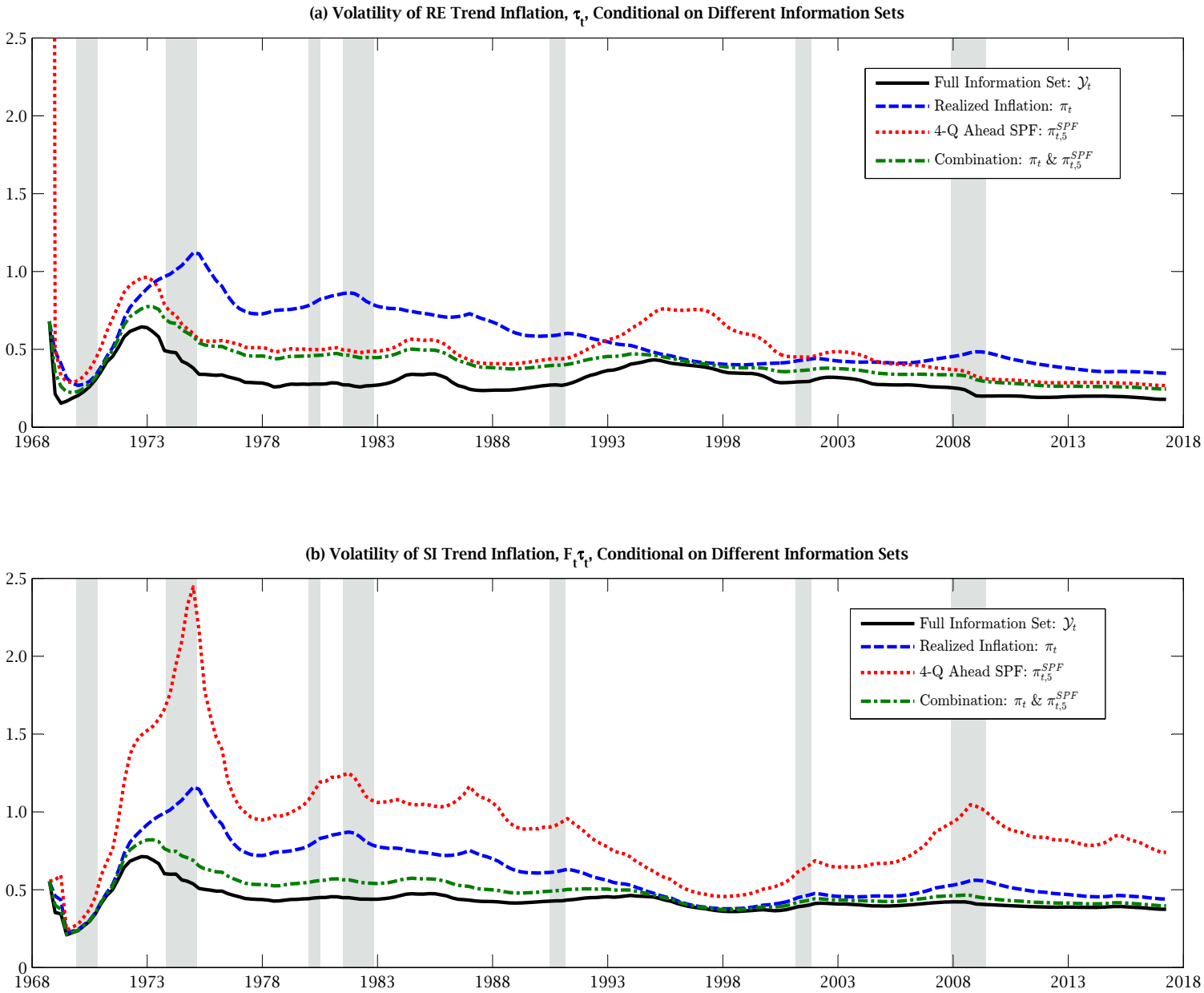

Note: The volatilities of RE and SI inflation trend are estimated in a joint DGP in which gap inflation, ε_t, has no persistence. The two plots contain vertical gray bands that denote NBER dated recessions.

A4.2 Estimates of the Joint DGP when $\lambda_t = \lambda$

Fixing the SI parameter generates estimates of the joint DGP that differ only along one dimension compared with the joint DGP of the SI-prediction mechanism and SW-UC-SV-TVP-AR(1) model. The difference is the minimal fluctuations of σ_η^2, σ_υ^2, and σ_ϕ^2 displayed in figure A2–$\widehat{\lambda}$, which repeats the theme of the plots presented in figure A2-No Gap Persistence. Otherwise, the joint DGP with $\lambda_t = \lambda$ is responsible for $\tau_{t|t}$, $F_{t|t}\tau_t$, $\varepsilon_{t|t}$, and $F_{t|t}\varepsilon_t$ (see figure A3–$\widehat{\lambda}$), of $\varsigma_{\eta,t|t}$, $\varsigma_{\eta,t|T}$, $\varsigma_{\upsilon,t|t}$, and $\varsigma_{\upsilon,t|T}$ (see figure A4–$\widehat{\lambda}$), of $\theta_{t|t}$, $\theta_{t|T}$, $|\theta_{t|T}|$, and $|\theta_{t|T}| - |\theta_{1|T}|$ (see figure A5–$\widehat{\lambda}$), and of the volatility of τ_t and $F_t\tau_t$ against disparate information sets (see figure A7–$\widehat{\lambda}$) that give evidence about the stickiness, persistence, and volatility of π_t and $\pi_{t,t+h}^{SPF}$ that support the results and interpretation reported by the paper.

This section concludes with a figure that plots the PLE path of $\widehat{\lambda}$. The PLE path of $\widehat{\lambda}$, 68 percent uncertainty bands, and 90 percent uncertainty bands appear in Figure–$\widehat{\lambda}$. This figure shows that by the end of the 1973–1975 recession the PLE path of $\widehat{\lambda}$ displays smaller fluctuations and from 1988 to the end of the sample exhibits almost no movement settling around 0.30 with 95 percent uncertainty bands ranging from 0.25 to 0.36. The dearth of movement in the PLE path of $\widehat{\lambda}$, especially after 1988, is a reason the data prefer the joint DGP of the SI prediction mechanism and SW-UC-SV-TVP-AR(1) model.

Figure A2–$\hat{\lambda}$: Estimates of Static Volatility Parameters, 1968$Q4$ to 2017$Q2$

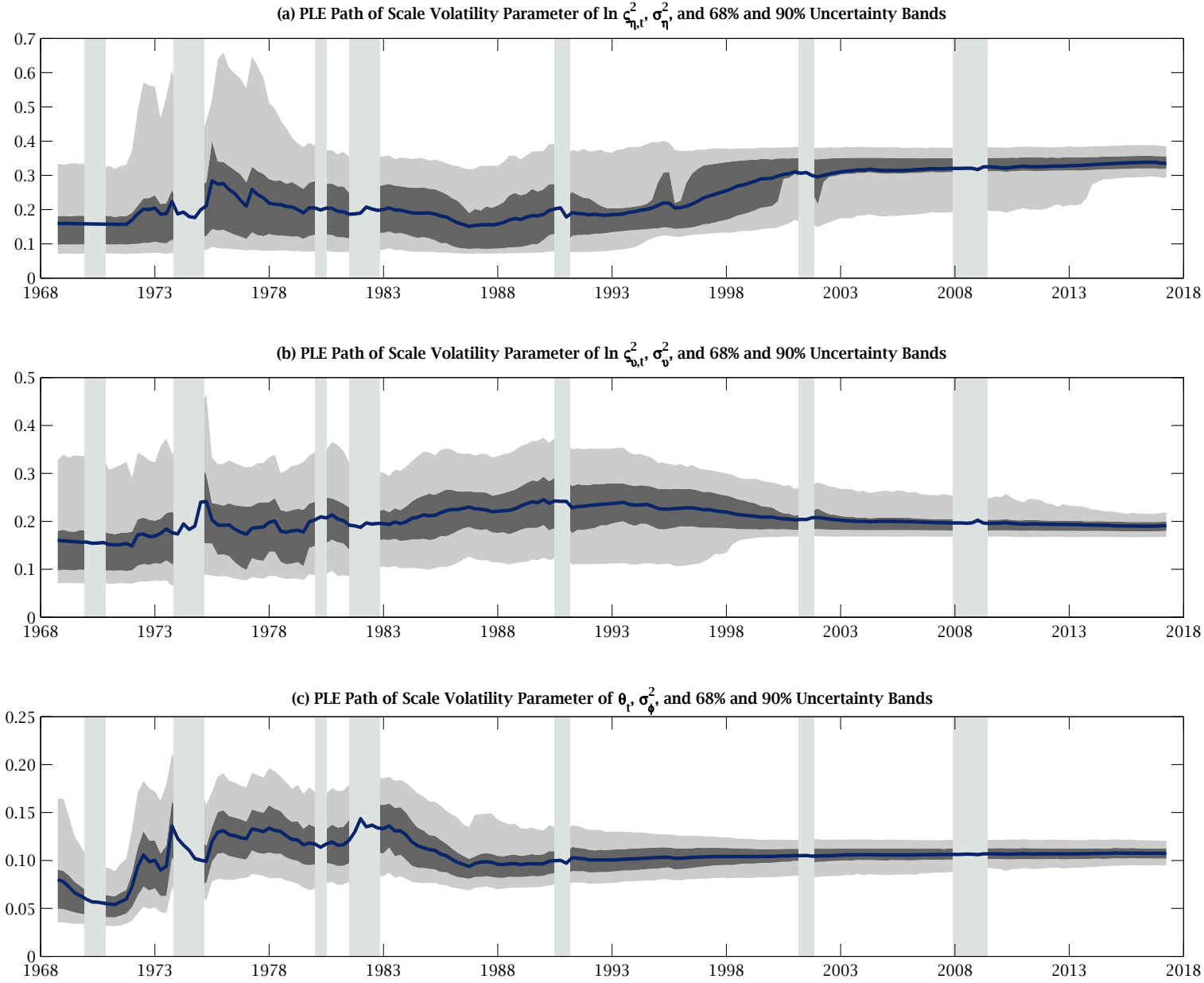

Note: The static volatility parameters are estimated in a joint DGP that has a static SI parameter, $\lambda_t = \lambda$. The dark (light) gray areas surrounding estimates of the static scale volatility parameters, σ^2_η, σ^2_υ, and σ^2_ϕ cover 68 (90) percent uncertainty bands. The four plots contain vertical gray bands that denote NBER dated recessions.

Figure A3-$\hat{\lambda}$: Realized Inflation, SPF Inflation Predictions, and Estimates of Trend and Gap Inflation, 1968$Q4$ to 2017$Q2$

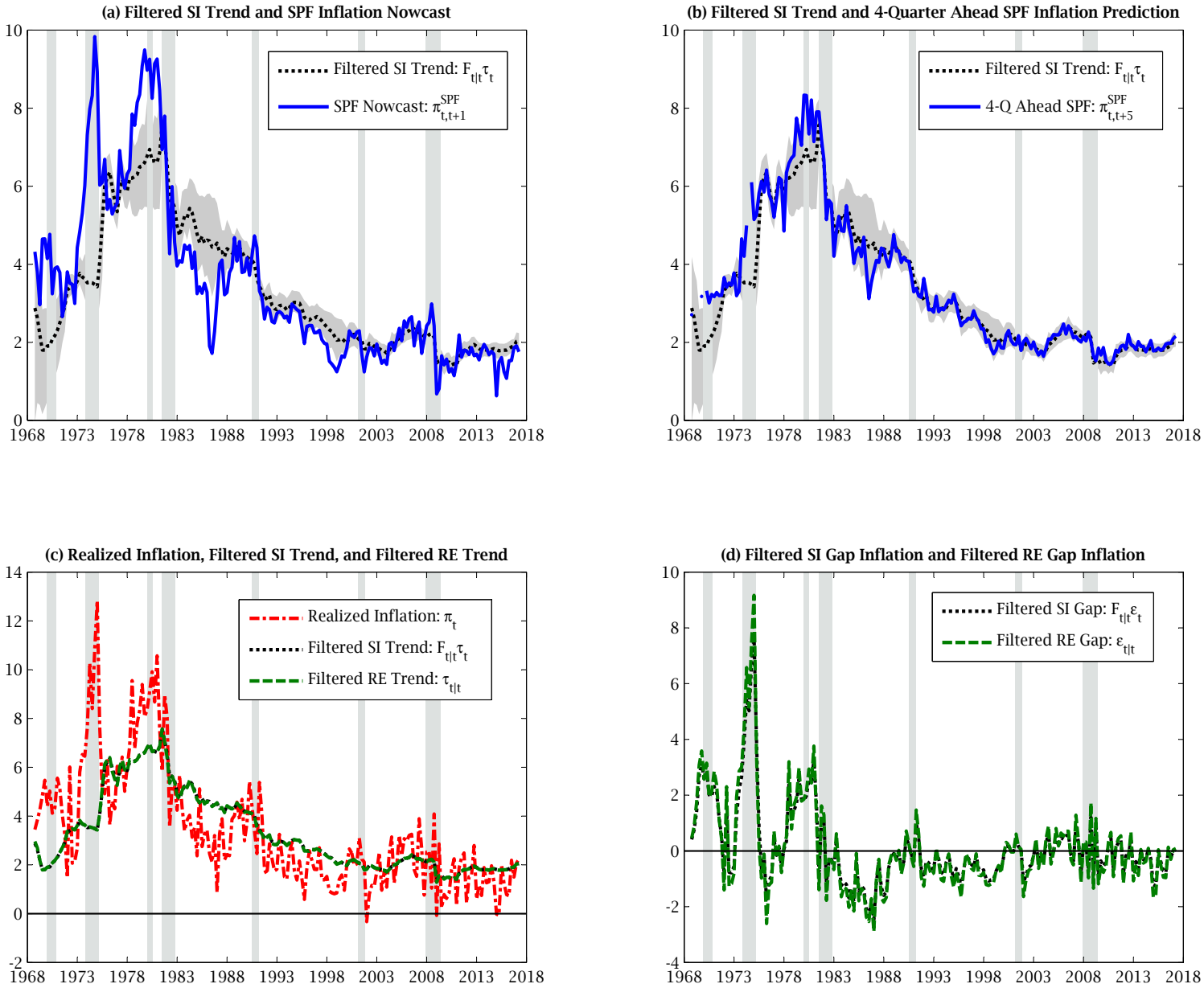

Note: The filtered RE and SI inflation trends and gaps are estimated in a joint DGP that has a static SI parameter, $\lambda_t = \lambda$. The top row of charts contains light gray shaded areas that represent 68 percent uncertain bands around estimates of filtered SI trend inflation, $F_{t|t}\tau_t$. The vertical gray bands denote NBER dated recessions in the four charts.

Figure A4-$\hat{\lambda}$: Estimates of the Stochastic Volatility of Trend and Gap Inflation, 1968$Q4$ to 2017$Q2$

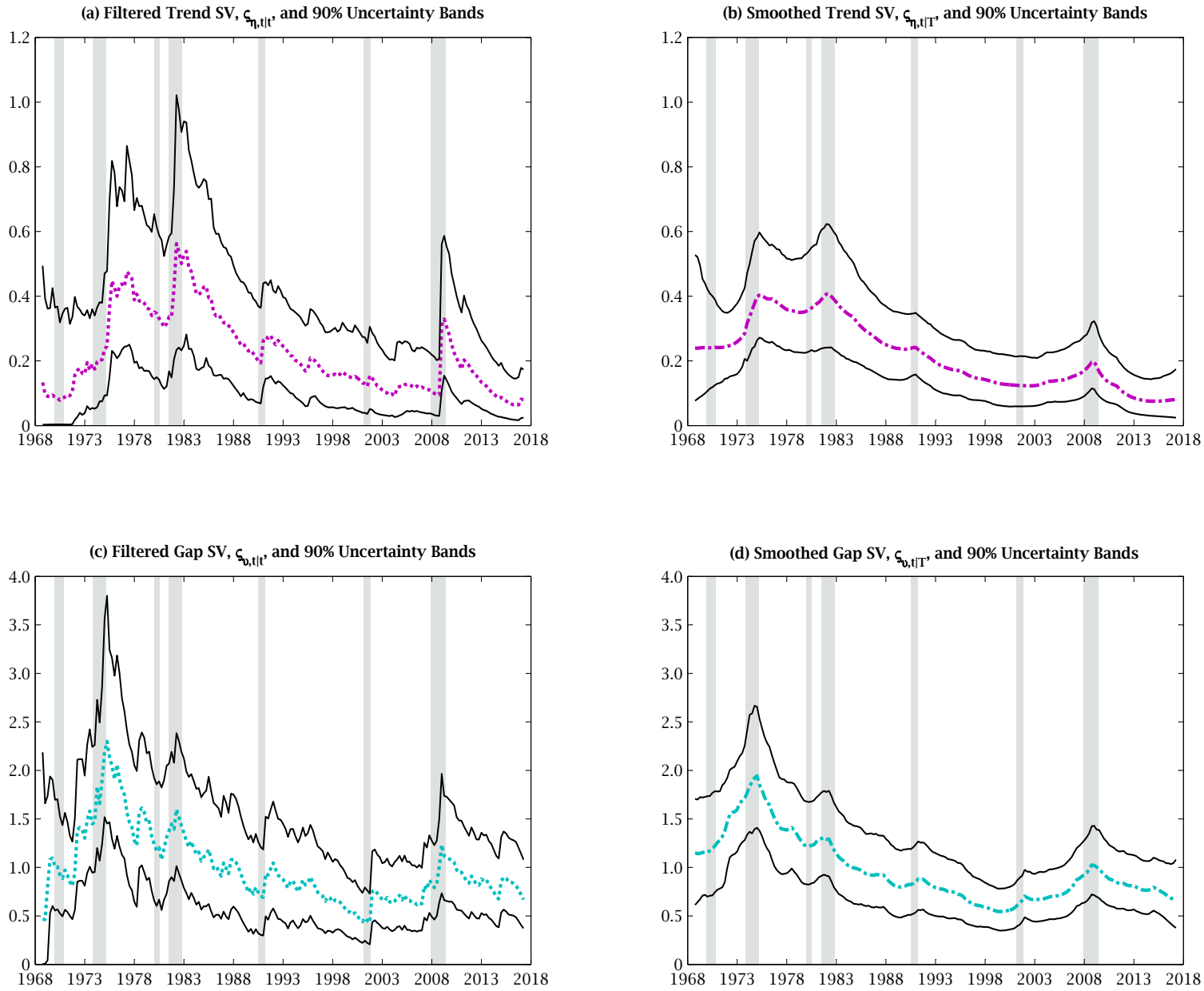

Note: The filtered and smoothed SVs of trend and gap inflation, $\varsigma_{\eta,t|t}$ and $\varsigma_{\eta,t|T}$, are estimated in a joint DGP that has a static SI parameter, $\lambda_t = \lambda$. The solid thin (black) lines around estimates of $\varsigma_{\eta,t|t}$ and $\varsigma_{\eta,t|T}$ are lower and upper bounds on 90 percent uncertainty bands. The four plots contain vertical gray bands that denote NBER dated recessions.

Figure A5–$\hat{\lambda}$: Estimates of Time-Varying Inflation Gap Persistence, 1968Q4 to 2017Q2

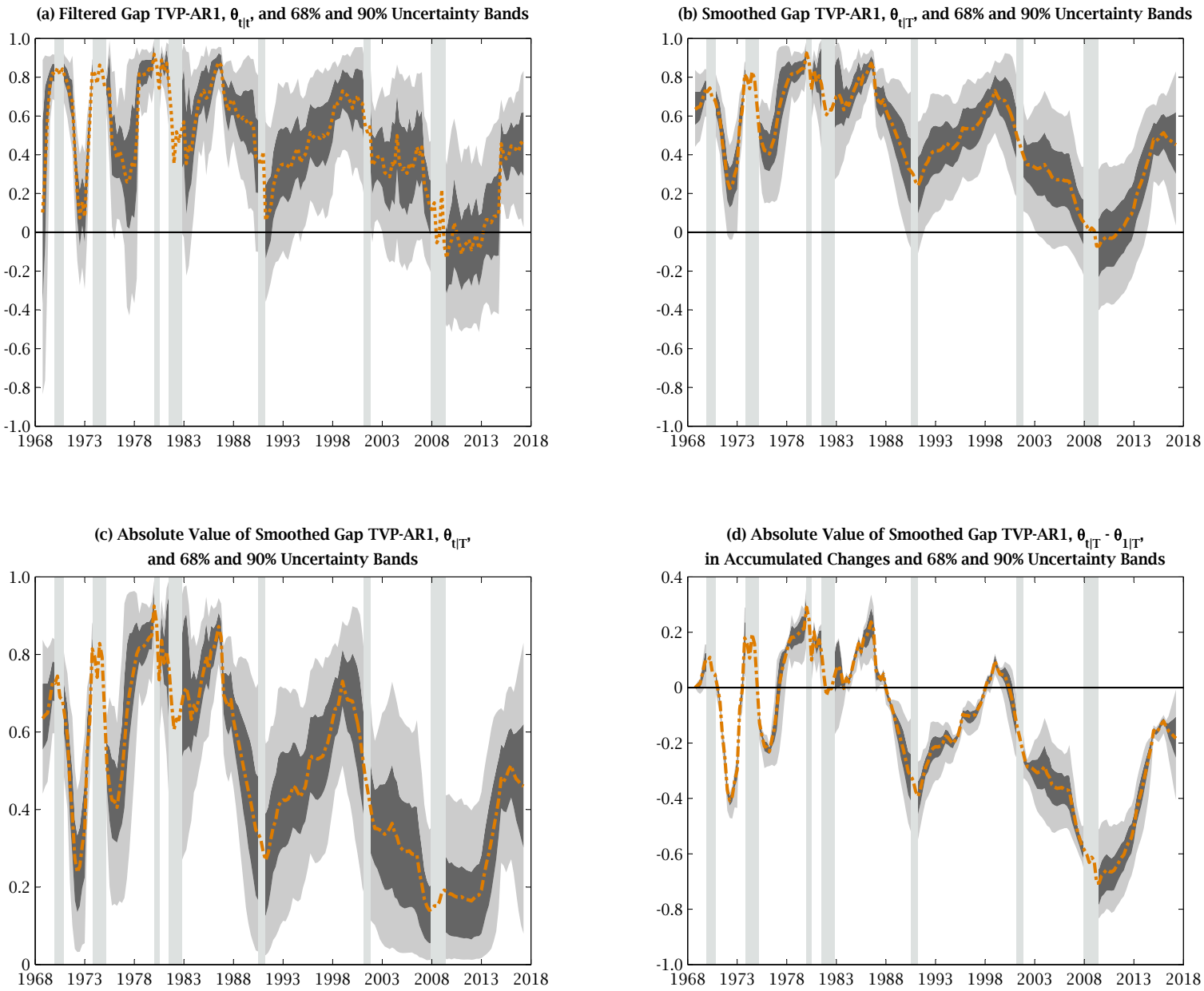

Note: The filtered and smoothed TVP-AR1 parameter of gap inflation is estimated in a joint DGP that has a static SI parameter, $\lambda_t = \lambda$. The dark (light) gray areas surrounding estimates of the TVP-AR1 of gap inflation cover 68 (90) percent uncertainty bands. The four plots contain vertical gray bands that denote NBER dated recessions.

Figure A7-$\hat{\lambda}$: Uncertainty Measure of Trend Inflation Conditional on Different Information Sets, 1968$Q4$ to 2017$Q2$

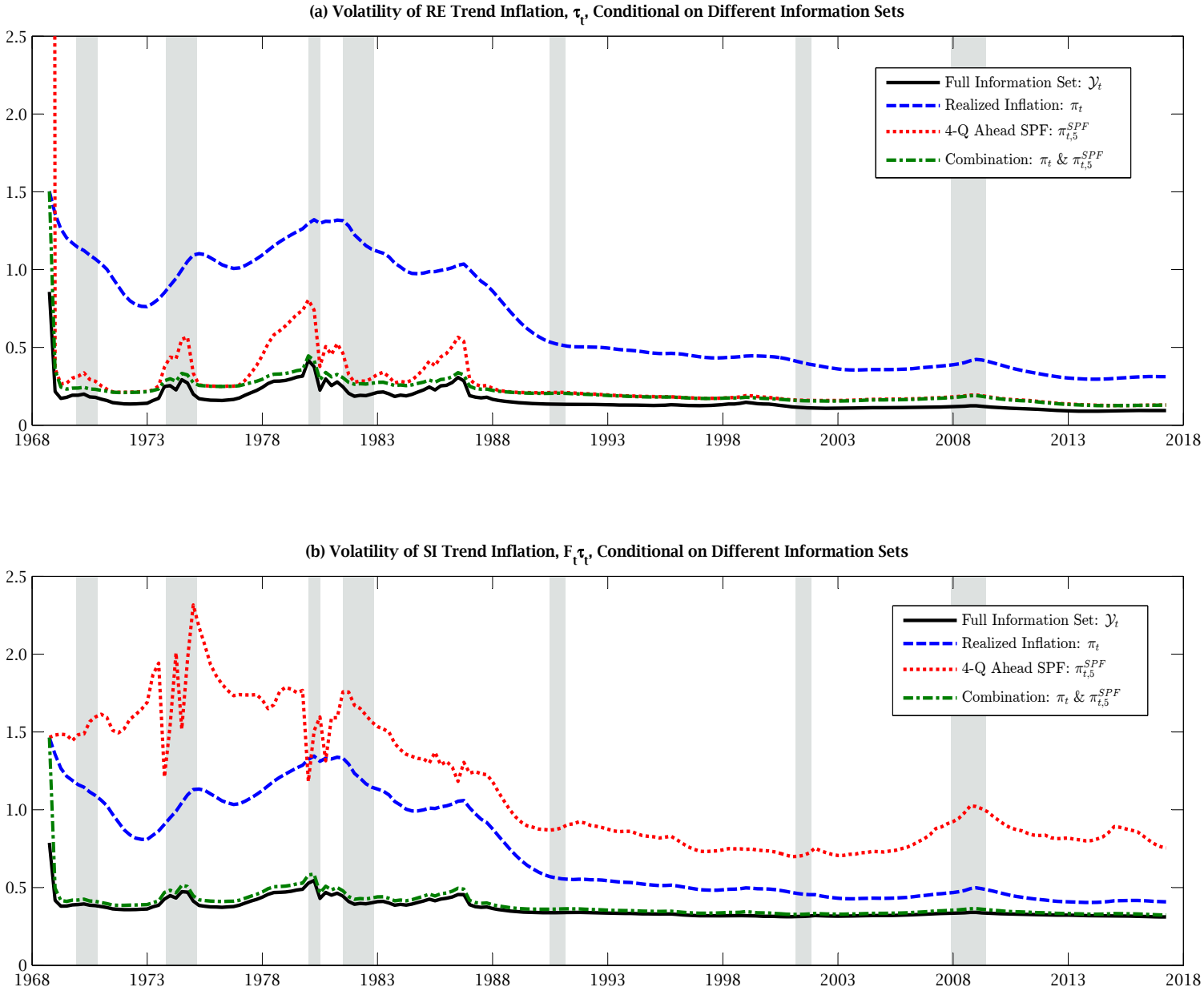

Note: The volatilities of RE and SI inflation trend are estimated in a SW-UC-SV model in which the SI parameter is static, $\lambda_t = \lambda$. The two plots contain vertical gray bands that denote NBER dated recessions.

Figure–$\widehat{\lambda}$: Particle Learning Estimates of the Static SI Parameter, λ, $1968Q4$ to $2017Q2$

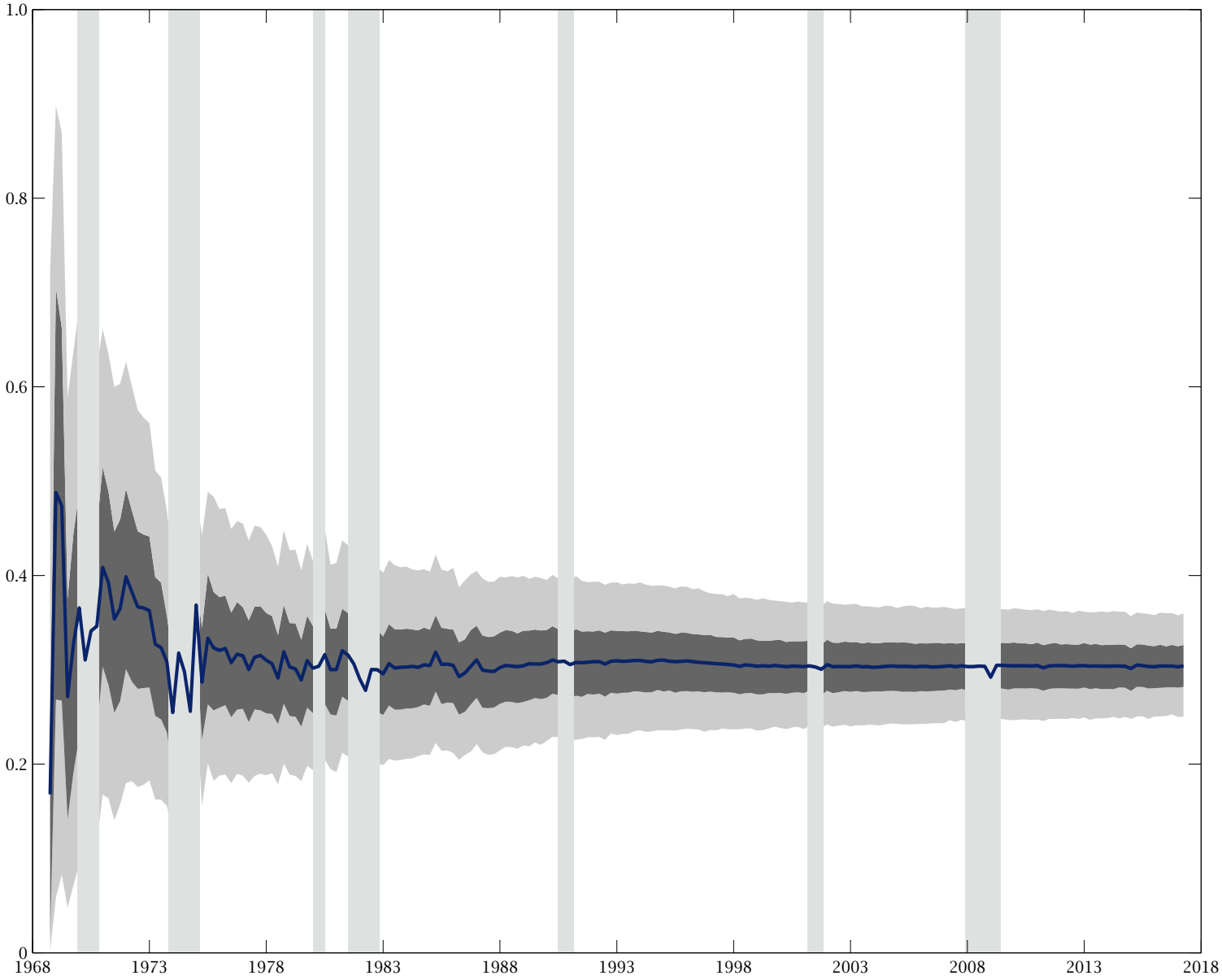

Note: The PLE estimates of λ are the solid blue line. The dark (light) gray areas surrounding estimates of λ cover 68 (90) percent uncertainty bands. The figure also has vertical gray bands that denote NBER dated recessions.

References

Carvalho, C.M., M.S. Johannes, H.F. Lopes, and N.G. Polson (2010). Particle learning and smoothing. *Statistical Science* 25, 88–106.

Creal, D. (2012). A survey of sequential Monte Carlo methods for economics and finance. *Econometric Reviews* 31, 245–296.

Hol, J.D., T.B. Schön, F. Gustafsson (2006). On resampling algorithms for particle filters. In 2006 IEEE NONLINEAR STATISTICAL SIGNAL PROCESSING WORKSHOP, Ng, W. (ed.), 79–82. Red Hook, NY: Curran Associates, Inc.

Lindsten, F., P. Bunch, S. Särkkä, T.B. Schön, S.J. Godsill (2016). Rao-Blackwellized particle smoothers for conditionally linear Gaussian models. *IEEE Journal of Selected Topics in Signal Processing* 10, 353–365.

Lopes, H.F., R.S. Tsay (2011). Particle filters and Bayesian inference in financial econometrics. *Journal of Forecasting* 30, 168–209.

Pitt M.K., N. Shephard (2001). Auxiliary variable based particle filters. In SEQUENTIAL MONTE CARLO METHODS IN PRACTICE. Doucet, A., de Freitas, N., Gordon, N. (eds.). New York: Springer-Verlag.

Pitt, M. K., N. Shephard (1999). Filtering via simulation: auxiliary particle filters. *Journal of the American Statistical Association* 94, 590–599.

Storvik, G. (2002). Particle filters for state-space models with the presence of unknown static parameters. *IEEE Transactions on Signal Processing* 50, 281–289.